Strong-Field Excitation of Liquid and Solid Xe Using Intense Femtosecond Pulses[†]

M. Pettersson,[‡] R. Zadoyan,[§] J. Eloranta, N. Schwentner,[∥] and V. A. Apkarian*

Department of Chemistry, University of California, Irvine, California 92612-2025

Received: December 20, 2001; In Final Form: February 22, 2002

Strong-field excitation of condensed xenon, both solid and liquid, are investigated using focused 60 fs pulses at 400 and 800 nm. Both wavelengths lead to efficient generation of excitons, which are monitored through their VUV emissions. The self-trapped Xe_2^* excitons are observed in both solid and liquid Xe; and although weaker, emission from the free Xe^* excitons is also detected in the crystalline samples. The photoionization mechanism, which ultimately leads to the creation of excitons through electron−hole recombination, is investigated through power dependence measurements of fluorescence and transmission. At 400 nm, the ionization proceeds through the multiphoton mechanism, while at 800 nm, field-induced tunneling ionization prevails. It is observed that the ionization process is self-limited, preempting the possibility of dielectric breakdown. The failure of an electron avalanche process to develop is understood to arise from the small scattering cross-section of electrons in condensed Xe whereby the field-driven electron energy distribution localizes at the deep scattering minimum, near 0.7 eV. Additionally, the achievable field intensities are limited by beam divergence, due to the negative refraction in the generated electron plasma. This is established in the liquid-phase samples by transmission measurements through a limiting aperture. In the solid state, damage triggered by defects limit the achievable irradiation intensities. It is estimated that exciton densities of $\sim10^{18}$ cm^{-3} are reached (at pump intensities of 10^{12} W/cm^2). Although amplification of stimulated emission can be expected at the achieved number densities, no evidence of gain is found in the on-axis spectral profile of the excitonic emission.

I. Introduction

With the accessibility of lasers with ultra-short pulses, the investigation of systems under strong-field irradiation conditions has become an important area of research. The readily available intensities on the order of $10^{12}-10^{16}$ W/cm^2 lead to significantly new routes to highly excited states of matter.[1,2] At intensities where the electric field of the radiation approaches and exceeds the nuclear Coulombic potential, field-induced ionization of atoms via tunneling,[3] or complete Coulomb barrier suppression,[4] occurs. En route to ionization, coherently driven Rydberg electrons serve to generate high harmonics of the field, leading to the production of X-ray[5] and attosecond pulses.[6] In molecular systems, strong-fields allow controlled manipulations,[7] with examples ranging from selective ionization and controlled fragmentation,[8,9] to the more gentle field-driven molecular centrifuge.[10] There are important differences between such applications in the gas phase versus condensed media. Collective dynamics of electrons already appear in the bridging studies of clusters, where intense short pulses give access to highly ionized states of atoms, such as Xe^{20+} and I^{17+},[11,12] leading in the extreme limits to laser fusion.[13] In bulk applications, the important distinctions arise from the characteristically nonlinear propagation of intense pulses.[14] This is familiar in such practical applications as supercontinuum generation[15] or ablation,[16] and clearly must play an integral part in the design of controlled

molecular dynamics in condensed media. In this regard, studies in condensed rare gases are useful, since they allow the isolation of field-matter nonlinearities to strictly electronic degrees of freedom. In a previous work in superfluid helium, we provided a detailed description of the processes involved in strong-field-induced ionization, from the limit of a controlled ionization cascade to produce XUV excitations to the dissection of breakdown.[17] Moreover, below the breakdown threshold, third harmonic generation could be seen, and has since been characterized in greater detail.[18] These observations provide a measure of the coherence in the field-driven Rydberg electrons, the limits of which have not yet been fully explored. In the present work, we extend the concepts and methods to investigations in solid and liquid Xe. In particular, we consider strong-field pumping as a means to access the excitonic states of Xe which lie in the VUV, and we consider the possibility of pumping an excitonic laser by this approach.

Impurity-doped rare gas solids and liquids offer the simplest environment to investigate processes in the condensed phase, and they have been successfully used to understand principles of condensed-phase photodynamics.[19] The spectroscopy and dynamics of pure condensed rare gases have attracted significant interest and remain active areas of research.[20−24] Due to their large band gap, traditionally, synchrotron radiation and electron beam pumping have been used to reach the excited states. The time resolution offered by these methods is limited to the nanosecond or picosecond regime; accordingly, mostly information concerning the trapping dynamics of free excitons has been obtained.[25−28] Details of many elementary processes remain less clear. Examples include: the decoherence of free excitons, their mobility, trapping, and ionization, and subsequent relaxation dynamics of excitons, electrons, and holes. Given an ultrafast

Strong-Field Excitation of Liquid and Solid Xe

J. Phys. Chem. A, Vol. 106, No. 36, 2002 **8309**

method for preparing the excitons, significant progress in our understanding of these fundamental processes can be expected, as has already been demonstrated in supercritical Xe by using picosecond pulses.[29] Historically, the investigation of radiative properties of pure condensed rare gases was motivated by the prospects of developing a VUV excimer laser.[30] The report by Basov et al.[31] of laser action in electron beam pumped liquid Xe led to a frenzy of activity, which resulted instead in the well-established science and technology of gas-phase, rare gas halide exciplex lasers.[32] Despite significant efforts, the efficiencies obtained in electron-beam pumped gaseous and liquid neat rare gases remained too low for the practical construction of a working laser.[31,33−35] A significant effort has been expended in electron beam-pumped crystalline rare gases for the same purpose, and while excitation densities sufficient to obtain gain were reached in careful studies, net gain remained illusive due to losses ascribed to transient absorption.[36] In contrast, large gain and laser action has been demonstrated in optically pumped, doped rare gases both in the liquid phase[37] and in the solid state.[38,39] Thus, given an efficient optical pumping scheme of the neat, condensed rare gases, their gain characteristics could be reevaluated.

In what follows, we describe experiments in which 60 fs laser pulses, at 800 nm and at 400 nm, are used to pump liquid Xe and free-standing crystals of Xe. We follow the excitonic emissions in the VUV to understand the highly nonlinear mechanisms of strong-field pumping. We discover that field-induced ionization in this system is self-limiting, precluding the possibility of breakdown and potentially the achievable number densities of excitons in arbitrary excitation geometries. Thus, we recognize the importance of characterizing nonlinear refraction in such applications, and provide an analysis of power-dependent transmission, and fluorescence.

II. Experimental Details

Both free-standing crystals and liquid Xe were investigated. Free-standing Xe crystals were grown from Xe gas (Matheson 99.997%) at a backing pressure of ∼160 mbar. The sample preparation took about 30 min and resulted in an optically clear crystal with dimensions of about 1 cm × 1 cm × 1 cm. Some light scattering at the surface was evident by eye after retracting the mold. The cryostat was equipped with a LiF window for the measurement of VUV emission. In some experiments, nominally pure Xe was further purified from water and oxygen by a Hydrox purifier (Matheson), or by γ-irradiation of the gas over the period of several days. In the solid-state measurements, trace amounts of water lead to strong fluorescence from the charge transfer states of H, near 250 nm, and of O, near 750 nm. Liquid measurements were done in a "T"-cell, equipped with a 1 mm-thick sapphire entrance window and a 3 mm-thick MgF_2 output window. The optical path length between entrance and exit windows of the cell was 2 cm. The temperature of the liquid was held at 167 ± 3 K during the measurements. While the majority of solid-state measurements were carried out at 15 K, in spectral narrowing measurements temperatures as high as 60 K were studied.

Femtosecond pulses were generated from a Ti:sapphire oscillator pumped with an argon-ion laser, followed by a stretcher, regenerative amplifier pumped by a YAG laser, and a grating compressor. Either the fundamental (800 nm) or the second harmonic (400 nm, generated using a BBO crystal) of the laser were used in the experiments. The temporal width of the pulse was determined with an auto-correlator to be 60 fs fwhm (assuming the pulse to be Gaussian in time). The laser
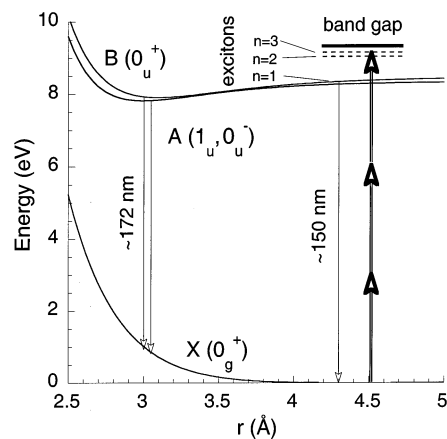

Figure 1. Schematic representation of the molecular states of Xe_2 and band states of solid Xe. The transitions from the A and B states to the ground state at 172 nm correspond to emission from the self-trapped excitons in condensed Xe. The energy of 400 nm photons is represented by the up-arrows, indicating that minimally three photons are required for excitation. The ∼150 nm transition, which is observed in solid Xe, corresponds to emission from free excitons. The diatomic gas-phase potentials are taken from refs 40 and 41, and the band state energetics is taken from ref 22.

beam was focused using a lens with focal length of either 20 or 14 cm. The spatial profile of the beam waist for the 400 nm pulses was characterized in air, using a 1 μm pinhole mounted on an $x-y-z$ translation stage. The profile was fitted to a Gaussian, to obtain a 1/e width at the focal plane of 33 ± 5 μm and 25 ± 5 μm for the longer and shorter focal length lenses, respectively. The excitation volumes and intensities are estimated using these values.

Emission from the samples, from VUV (∼140 nm) to near-infrared (∼800 nm), was dispersed through a monochromator (McPherson), using different gratings and photomultipliers (Hamamatsu, R331, R166UH, R1220). For measurements below 200 nm, the monochromator and the space between the slit and the window of the cryostat were purged with Ar gas. In measurements of emission collinear with the excitation beam, to block the pump beam a broadband VUV filter (Acton) with a transmission maximum at 180 nm was used.

The power-dependencies of the emissions were measured using a variable neutral density filter to attenuate the pump beam. In free-standing crystals, the measurements were complicated by the irreversible processes of laser-induced accumulation of defects and damage. To test repeatability, emission intensities were measured in a given spot as a function of both increasing and decreasing laser intensity. Only measurements showing reversibility of fluorescence intensity were retained. The 800 nm excitation results were highly irreproducible in the solids; therefore, we report only the 400 nm data. The liquid-phase results were perfectly reproducible for both 400 and 800 nm excitation. In addition to emission, transmission measurements were carried out in the liquid. This was accomplished using a photodiode placed on axis, behind a limiting aperture to monitor variations in the beam divergence due to nonlinear photorefraction.

III. Experimental Results

A. Spectral Observations. The potential energy curves of Xe_2^* ($X0_g^+(^1\Sigma_g^+)$), $A1_u$, $0_u^-(^3\Sigma_u^+)$, and $B0_u^+(^1\Sigma_u^+))$,[40,41] and the excitonic levels of solid Xe which are relevant to this work, are shown in Figure 1. Upon 400 or 800 nm excitation of either crystalline or liquid Xe, strong emission in the 170−180 nm
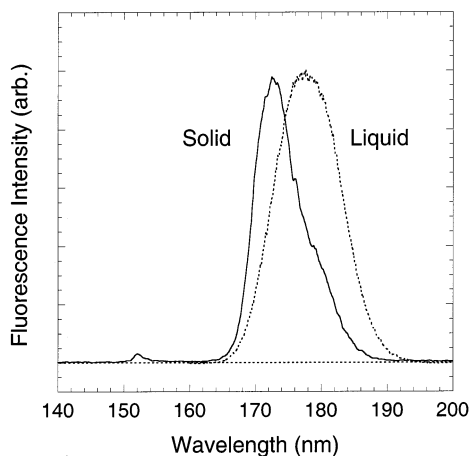
Figure 2. The observed emission bands in solid and liquid Xe under 400 and 800 nm excitation. The solid-state emission spectrum shows a strong band at 172 nm due to the emission from the self-trapped excitons (Xe_2^*) and a weak band at ~150 nm corresponding to emission from the free exciton. The liquid spectrum contains emission only from the Xe_2^*. The solid-state spectrum is from a free-standing crystal at a temperature of 15 K and the liquid spectrum is recorded at 170 K.

region is observed, as illustrated in Figure 2. In the solid state an additional weak band occurs at ~150 nm (see Figure 2). The bands centered at 172 and 178 nm are well established to originate from overlapping A → X and B → X transitions of the Xe_2^* excimer (or equivalently, the self-trapped exciton) in condensed Xe. The weak band at 152 nm in solid Xe is assigned to emission from the free exciton. [20-24]

Various observations concerning the spectroscopy of the excitons were made which are essentially in agreement with the existing literature.[20-25] In both solid and liquid, the Xe_2^* emission at ~170−180 nm shows two different decay components. The shorter component was instrument limited to less than 5 ns, in both liquid and solid. The longer component decays with a time constant of 100 ns in crystalline Xe at 15 K, and 25 ns in liquid Xe at 165 K. The previously observed temperature-dependence of the longer lifetime component was confirmed in our experiments.[42] The emission spectrum in crystalline Xe shows two spectral components centered at 172 and 178 nm, also in accordance with previous observations.[25,43] At 15 K, the 178 nm band decays with a lifetime of ~160 ns, and the 172 nm band decays with a lifetime of 100 ns. These two spectral components have been interpreted to originate from two different sites, the shorter wavelength component belonging to the exciton in a crystalline environment and the longer wavelength component belonging to excitons at defect sites. It has also been suggested that the emission at ~172 nm originates from excitons trapped at vacancies.[44,45] In our experiments, the ratio between the two components was approximately constant from experiment to experiment, and it did not change in the course of irradiation.

B. Power Dependencies. The energy of three 400 nm photons, or six 800 nm photons, is 9.3 eV, nearly coincident with the band gap of Xe at 9.33 eV.[22] In contrast, two photons at 400 nm (6.2 eV), or five photons at 800 nm (7.75 eV), remain well below the first exciton energy of 8.37 eV.[22] Therefore, in the perturbative limit, the observed VUV emissions can be expected to be induced via three-photon or six-photon processes with 400 and 800 nm pulses, respectively.

The observed dependence of the excitonic fluorescence intensity on pump intensity is presented in Figures 3 and 4, for 400 nm excitation of crystalline and liquid Xe, respectively. In both cases, the log−log plots show an initial linear regime, over
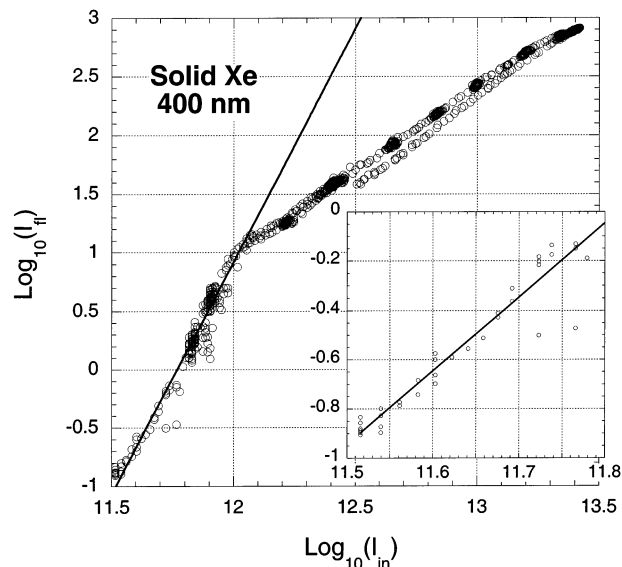

Figure 3. The power-dependence of the fluorescence from self-trapped excitons, Xe_2^*, in solid Xe pumped at 400 nm. The data are shown as a log−log plot, the abscissa being the decadic logarithm of the intensity in W/cm^2 that would be achieved at the focal point in air. The data are recorded from the same spot, first as the pump intensity is increased, and then as it is decreased, to verify reproducibility. The inset shows the linear fit in the first decade in fluorescence to have a slope of 3.
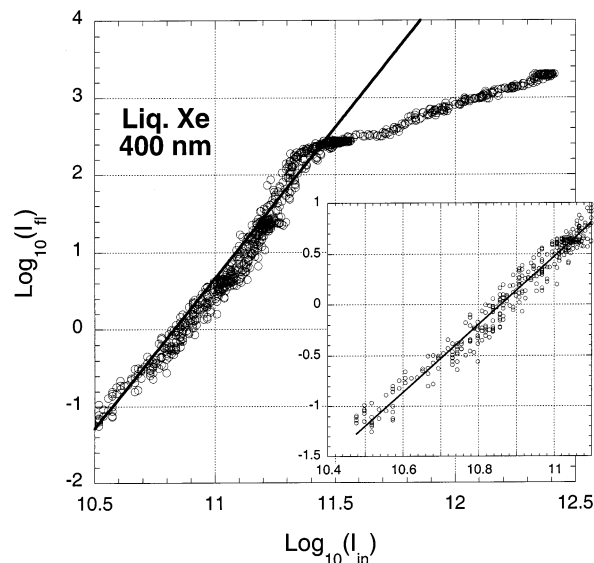

Figure 4. The power-dependence of the fluorescence from self-trapped excitons, Xe_2^*, in liquid Xe pumped at 400 nm. The construction of the plot is the same as in Figure 3. The linear fit to the first two decades in fluorescence gives a slope of 3.4.

2−3 decades in emission, followed by saturation. Expansions of the linear regime are shown as insets, in which the best-fit lines are also included. The first decade in emission in the solid state shows a linear dependence with a slope of 3 (see inset to Figure 3). Similarly, the first two decades in emission in the liquid phase fit a line with a slope of 3.4 (see inset to Figure 4). The saturation regime is characterized by a power dependence of 1 in the liquid and 1.4 in the solid. The liquid-phase data clearly show that saturation is preceded by nonlinearity in the logarithmic plot, where the slope of the dependence initially increases and then turns over.

That the propagation of the intense pulses in the liquid phase is subject to nonlinear refraction is most clearly illustrated by the transmission data obtained at 400 nm, in liquid Xe, which
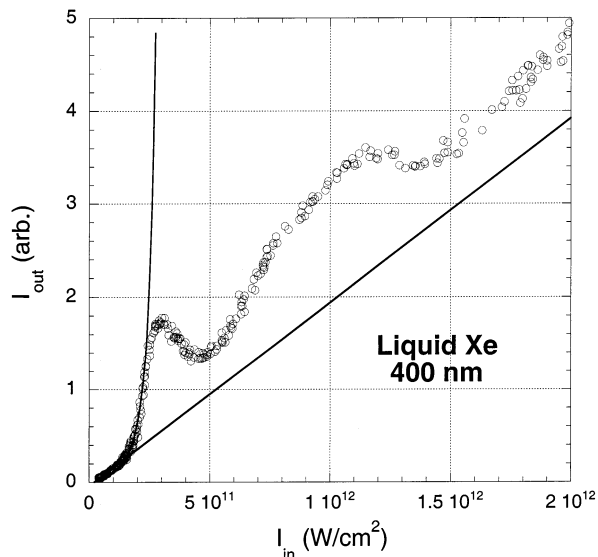
Strong-Field Excitation of Liquid and Solid Xe

J. Phys. Chem. A, Vol. 106, No. 36, 2002 **8311**

Figure 5. Power dependence of transmission at 400 nm in liquid Xe, observed through a pinhole. The initial points are extrapolated to show the linear limit. The curve fit is for self-focusing according to eq 13 of text.

Figure 6. The power-dependence of the fluorescence from self-trapped excitons, Xe_2^*, in liquid Xe pumped at 800 nm. The expected power law for multiphoton excitation would have a slope of 6, as indicated. The observed data fit a power law of 25, indicating field-induced tunneling ionization as the mechanism of excitation.

is collected in Figure 5. These measurements were carried out with a limiting aperture; hence, they are sensitive to the sum of real and imaginary parts of the nonlinear susceptibility in the medium. The data are shown along with the linear limit defined by the initial points. The transmitted intensity initially rises, indicating self-focusing. Then, at the nominal input intensity of 3×10^{11} W/cm^2 the transmitted intensity falls toward the linear limit, indicating self-defocusing. This is repeated with a gentler dependence near the nominal input intensity of 1.2×10^{12} W/cm^2. The strong self-lensing, along with the knowledge that the excitation source has multiple transverse modes, are the reasons for which the reported excitation intensities must be regarded as nominal. The reported values are based on the intensity of the laser at its beam waist, in air.

The power dependence of the excitonic fluorescence in liquid Xe, induced by pumping at 800 nm, is shown in Figure 6. The behavior can be characterized as a threshold process. Immediately above the noise floor, the fluorescence grows with a slope of 25 in the log−log plot. This is followed by a sudden saturation, where the slope reaches a value of 1. The saturation coincides with white light generation and a strong attenuation in transmission. The transmission data is shown in Figure 7.

Laser breakdown, which would be evidenced by a visible spark at the focal waist, could not be induced in liquid Xe, neither at 400 nm nor at 800 nm, at intensities as high as 5×10^{13} W/cm^2 (20 μJ pulses focused through a lens with a focal length of fl = 14 cm).

Breakdown and permanent damage occurs in solid Xe, however, a definite threshold of the effect could not be established because of its poor reproducibility. In the solid state, the breakdown can be associated with the development of hot spots determined by both the intensity profile of the laser and defects in the solid, either preexisting or irradiation induced. The quality of the grown crystals is such that, typically, breakdown does not occur for intensities up to 2×10^{13} W/cm^2 (pulse-energies up to 10 μJ). Unless extensively prepurified, the propagating beam can be visualized in the free-standing crystals by the visible fluorescence from impurities such as oxygen. Visual inspection of such solids clearly indicate that the propagating radiation is self-trapped, usually as a single filament that travels the full 1 cm length of the crystal.
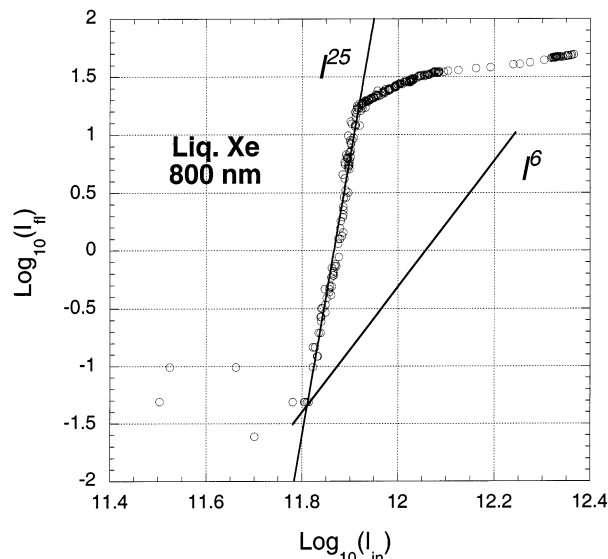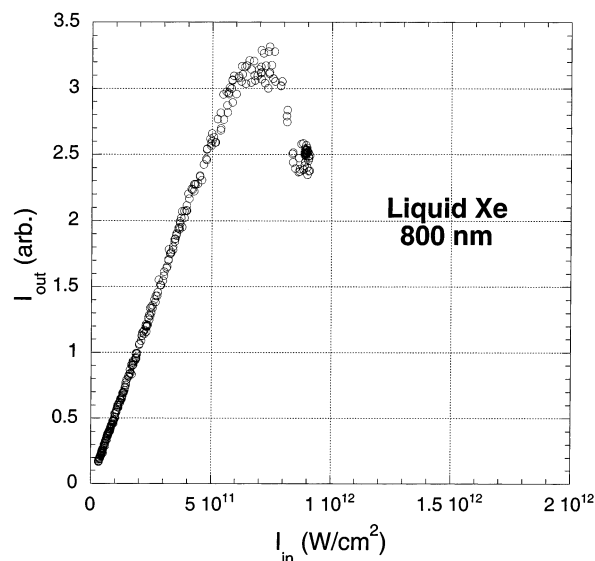

Figure 7. Power dependence of transmission at 800 nm in liquid Xe, observed through a pinhole. The drop in transmission occurs along with white light generation.

IV. Analysis & Discussion

A. Ionization Mechanism. The observed initial power dependence of excitonic emission induced by pumping at 400 nm is consistent with three-photon ionization followed by electron−hole recombination. At 800 nm, six photons would be required to reach the band gap in Xe. The observed power dependence of 25 in this case would indicate that strong-field ionization prevails over the six-photon process. The criterion for switchover between multiphoton ionization versus field-induced AC tunneling is given by the Keldysh adiabaticity parameter γ:[3]

$$\gamma = \frac{\omega\sqrt{\mu\Delta}}{eE} \qquad (1)$$

where ω is the laser frequency, μ the reduced mass of the electron−hole pair, Δ is the band gap, and E the electric field

amplitude of the pulse. The multiphoton regime corresponds to $\gamma > 1$, whereas tunneling ionization is expected for $\gamma < 1$. For a band gap of 9.3 eV, $\gamma = 1$ occurs at intensities of 5×10^{13} W/cm^2 and 1×10^{14} W/cm^2 for 800 and 400 nm pulses, respectively. Consistent with this, the multiphoton process is observed for the 400 nm excitation at nominal intensities below 10^{12} W/cm^2, for $\gamma > 10$.

In the case of 800 nm excitation, the very steep power dependence betrays tunneling field ionization, and this occurs in the narrow range of $8 < \gamma < 9$. The Keldysh criterion of eq 1 is useful for order of magnitude estimates, and is known to predict a higher switchover intensity than observed experimentally.[46] For example, the rare gas atoms are observed to undergo tunneling ionization in the gas phase for $1 < \gamma < 8$.[47] It is also useful to note that if we consider the primitive model for suppression of the Coulombic barrier by the laser field (electron subject to potential $V = -e^2/r - eEr$), the threshold intensity $I = E^4/16 = 3 \times 10^{13}$ W/cm^2 would be predicted.[4] The observed field-induced ionization at 800 nm occurs at a nominal intensity which is $\sim$50 times smaller than this limit (see Figure 6), and nearly 2 orders of magnitude smaller than intensities at which the first ionization of Xe saturates in the gas phase.[4] We may therefore conclude that the appearance of the excitonic fluorescence with 800 nm pumping is associated with the threshold for tunneling ionization. In the threshold region we would expect an exponential growth of ionization rate with pump intensity,[3] which is consistent with the observed steep power dependence of $\sim$25. The ionization process is, however, limited to a very narrow range in pump intensity, as evidenced by the observed abrupt turnover in the power dependence in Figure 6. Moreover, this turnover is directly correlated with the observations of white light generation and sharp drop in transmission (see Figure 7). The mechanisms that limit saturation of ionization, and therefore limit the attainable excitonic densities, deserve a deeper understanding. Key to this consideration is the feedback between nascent electrons and the propagation of the radiation field.

B. Kinetics of Field-Driven Electrons. A saturation effect is observed in all fluorescence measurements, whereby the initial power dependence reverts to nearly linear behavior. The turnover must be caused by the interaction of the pump field with the nascent electrons. Instead of this interaction leading to an electron avalanche and ultimate dielectric breakdown as it occurs in liquid helium,[17] here, a negative feedback occurs: the nascent electrons turn off further photoionization. To understand the qualitative difference between liquid He and liquid Xe, we model the electron dynamics with the same classical approach as in our previous work.[17]

Electrons created by photoionization are borne in an intense radiation field where they may be ponderomotively driven. In condensed media, in which scattering lengths are short, randomization of electron momenta upon scattering leads to heating. The electron kinetic energy distribution therefore evolves as a diffusion process along the energy axis, and when electrons reach the ionization limit of the host they may generate secondaries through impact.[48] The ionization dynamics during the laser pulse can be modeled by considering the time evolution of the electron energy distribution $f(\epsilon,t)$, by numerically solving the Fokker−Planck equation:[16]

$$\frac{\partial f(\epsilon, t)}{\partial t} = -\frac{\partial}{\partial \epsilon}\left[K_\epsilon(\epsilon)f(\epsilon, t) - D(\epsilon)\frac{\partial f(\epsilon, t)}{\partial \epsilon}\right] + S(\epsilon, t) \quad (2)$$

where $K_\epsilon(\epsilon)$ is the rate of energy gain by an electron in the radiation field, $D(\epsilon)$ is the energy diffusion coefficient, and $S(\epsilon,t)$ describes the sources and sinks of electrons, including
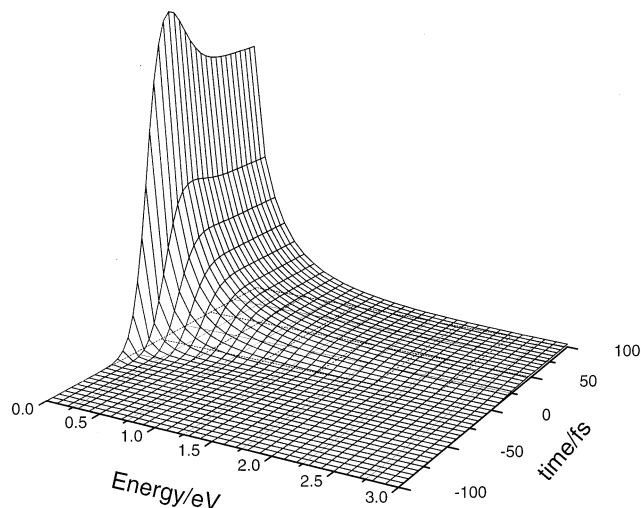

Figure 8. The evolution of the electron kinetic energy distribution function under the influence of a 400 nm laser pulse. The assumed laser pulse has a fwhm of 60 fs and peak intensity of 10^{14} W/cm^2, centered at $t = 0$. It is assumed that electrons are generated at zero energy through three-photon ionization by the laser pulse, and subsequently heated by the field. After termination of the pulse, practically no electrons have reached the ionization limit of 9.3 eV, precluding the possibility of an electron avalanche under these conditions.

photoionization and electron impact ionization. The rate for the n-photon ionization process is taken as

$$P^n(I) = \sigma^{(n)}\left(\frac{I}{\hbar\omega}\right)^n \rho \quad (3)$$

where I is intensity, $\sigma^{(n)}$ is the n-photon cross-section, and ρ is the density of the solid or liquid. The photoelectron distribution produced by the MPI is assumed to be a delta function at zero energy. We use the cross-sections $\sigma^{(3)} = 5 \times 10^{-81}$ s^2 cm^6 (and $\sigma^{(6)} = 1 \times 10^{-180}$ s^5 cm^{12}) which has been previously obtained in the gas phase for pulses at 248.6 and 586 nm.[49,50] $K_\epsilon(\epsilon)$ and $D(\epsilon)$ are determined by the momentum-transfer cross-section σ_{mt} in the condensed phase.[17] The latter is based on the gas-phase cross-section and the condensed-phase structure factor $S(\mathbf{K},\omega)$;[51,52] and has been verified to reproduce measured drift velocities of electrons in condensed rare gases.[53−55] We use the momentum-transfer cross-section calculated by Gushchin et al.,[54] which can be fitted to the functional form

$$\sigma_{mt} = 0.0295 + 0.1 \times (\epsilon + e^{-68.1\epsilon}) \quad (4)$$

with σ_{mt} given in Å^2 and energy ϵ in electronvolts. In going from the gas phase to the condensed phase, the scattering cross-section is reduced by more than 2 orders of magnitude in the relevant low energy regime. To describe the electron impact ionization process, the measured gas-phase cross-section was taken from Wetzel et al.[56] and adjusted by taking the band gap energy as the ionization threshold. The adjusted data was fitted to the functional form

$$\sigma_i = \frac{1}{\left(0.00576 + \frac{0.738}{\epsilon - 9.3}\right)\sqrt{\epsilon}} \quad (5)$$

where σ_i is in Å^2 and ϵ in eV.

The results of a typical evolution of the electron energy distribution function under 400 nm excitation is shown in Figure 8. In the simulation, as in the experiments, the temporal

Strong-Field Excitation of Liquid and Solid Xe

J. Phys. Chem. A, Vol. 106, No. 36, 2002 **8313**

evolution of the laser pulse intensity was described as a Gaussian with fwhm = 60 fs. In Figure 8, it can be seen that initially the distribution is zero everywhere. MPI feeds electrons at zero energy. After termination of the pulse, the distribution remains strongly peaked at energies below 1 eV. Practically, no electrons reach kinetic energies equal to the band gap. The same result is obtained with 800 nm pulses. In both cases, the slow electron heating rate is due to the small momentum-transfer cross-section and its functional dependence on energy. To be certain, we performed the same simulation using the gas-phase cross-section.[57] Even in that case the contribution of electron avalanche to the total electron density was negligible at intensities up to 10^{14} W/cm^2. The gas-phase simulations make it clear that the electron distribution localizes at the Ramsauer-Townsend minimum at ~0.7 eV, where the cross-section is again rather small (~1.2×10^{-16} cm^2),[57] being too small to lead to significant electron avalanche with 60 fs pulses. The overall conclusion from the simulations is that: with 60 fs pulses, ionization happens exclusively via the laser field, and secondary electrons do not contribute to any significant extent. Despite coupling of the radiation field to the plasma, the electron energy distribution after termination of the pulse remains peaked below ~1 eV. This is to be contrasted with the case in liquid helium.[17] There, the electron cascade rapidly develops into an avalanche at intensities and pulse widths similar to those used in the present simulation. The absence of a deep scattering minimum (due to the very small polarizability of He) in the scattering cross-section of electrons in helium is key to this difference. Here, the small scattering cross-section implies a slow diffusion of the electron distribution along the energy axis, which leads to trapping in the deep scattering minimum of the polarizable Xe.

The localization of the field-driven electron energy distribution at the scattering minimum is equivalent to nearly vertical stimulated absorption and emission processes. Accordingly, the observations that the turnover region is accompanied by attenuation of the pump and by white light generation can be understood, respectively, as net absorption and phase modulation of the radiation by the free electrons.[14] To be effective in this regard, the generated electron densities must be comparable to the photon flux near the turnover region. Estimates based on the nominal pump intensities and the MPI cross-sections are possible. Thus, for three-photon ionization in a medium characterized by the atomic density N:

$$\frac{dI}{dx} = -N\sigma^{(3)}I^{(3)} \tag{6}$$

which integrates to the form:

$$I_x = \sqrt{\frac{I_0^2}{2I_0^2 N\sigma^{(3)}\Delta x + 1}} \tag{7}$$

the pump intensity will drop to half its initial value over the length:

$$\Delta x_{1/2} = \frac{3}{2I_0^2 N\sigma^{(3)}} \tag{8}$$

At 400 nm, the turnover in the liquid is reached at an intensity of ~2×10^{11} W/cm^2 (see Figure 4). At which intensity over the length $\Delta x_{1/2} = 0.14$ cm (which is comparable to the Rayleigh length of $2\pi w_0^2/\lambda \sim 0.3$ cm, where w_0 is the radius of the beam in the focal plane in air), an electron density of 10^{17} cm^{-3}

develops. In the solid, at the same wavelength, the turnover occurs at a flux 10^{12} W/cm^2 yielding an electron density of 10^{19} cm^{-3} over a length $\Delta x_{1/2} = 45\ \mu$m. Note, in these estimates we have neglected self-lensing effects. This could explain the variation in the apparent electron densities at which we observe saturation. Self-focusing would imply that even larger electron densities are produced in the focal volume. We return to this consideration below. What is clear from the above analysis is that, in the absence of an electron avalanche, absorption by the photogenerated electrons can severely attenuate the pump beam, to reduce its intensity, effectively blocking further ionization of the host.

C. Self-Refraction. The transmission data obtained with a limiting aperture in the liquid phase studies allows the analysis of nonlinear refraction. The effect is negligible in the case of 800 nm pumping, where the transmission remains essentially linear until the limit of white light generation through self-phase modulation. In contrast, the transmission at 400 nm initially undergoes self-focusing then self-defocusing, with a milder repetition of the same process at higher intensity. The phenomenon of self-focusing is well understood.[14,58] It arises from the intensity-induced refractive index $n = n_0 + n_2 I$, due to the third-order nonlinear susceptibility present in all isotropic media: $n_2 = (12\pi^2/n_0\ c)\chi^{(3)}(\omega = \omega + \omega - \omega)$. Quite generally n_2 is positive in transparent materials, leading to a positive lens shaped by the transverse intensity profile of the beam. At 400 nm, the main contribution to the $\chi^{(3)}$ arises from the preresonance of the virtual two-photon excitation at $2\omega = 6.2$ eV with the first excitonic transition at 8.3 eV. It can be estimated from the frequency-dependent measurements of the hyperpolarizability of Xe that at 800 nm, $\chi^{(3)}$ is nearly three times smaller than at 400 nm.[59] This difference is evidently sufficient to reach tunneling ionization prior to significant self-focusing at 800 nm. Typically, self-focusing increases with intensity until reaching the diffraction limit, whereby filament formation (or self-trapping) takes over. In the present case, instead, we observe self-defocusing. What is required for this behavior to be observable is a negative dispersion, with intensity dependence that is steeper than that of self-focusing. This is to be expected from the contribution of the photogenerated electrons to the refractive index. Thus, upon ionization, the refractive index of the medium will change by the contribution from the free electron plasma:

$$\delta n_e(I) = 1 - \sqrt{1 - \frac{\omega_p^2(I)}{\omega^2}} \approx -\frac{1}{2}\frac{\omega_p^2(I)}{\omega^2} = -\frac{2\pi N_e(I)e^2}{m_e\omega^2} \tag{9}$$

where ω_p is the angular frequency of the plasma resonance, ω is the radiation frequency, m_e and e are the electron mass and charge, and N_e is the intensity-dependent electron density, and we have assumed that $\omega_p < \omega$. At the estimated electron number density of $N_e = 10^{18}$ cm^{-3} a plasma frequency of $\omega_p = 5.6 \times 10^{13}$ s^{-1} is to be expected, while the optical angular frequency is 4.7×10^{15} s^{-1} (400 nm). This leads to a reduction in index $\delta n_e = -7 \times 10^{-5}$ at the center of the beam. We may estimate the divergence angle due to this effect using Fermat's principle. We note that a central ray will travel a length $d' = c\Delta t/(n + \delta n)$ while a peripheral ray, at $r = w_0$ where the electron density becomes negligible, will travel a length $d = c\Delta t/n$ in the same time interval. The wave front will then tilt by an angle α, where

$$\tan(\alpha) = \frac{|d' - d|}{w_0} = \frac{d}{w_0}\left(\frac{1}{n + \delta n} - \frac{1}{n}\right)\left(\frac{\delta n}{n^2}\right) \approx \frac{d}{w_0}\left(\frac{\delta n}{n^2}\right) \tag{10}$$

8314 *J. Phys. Chem. A, Vol. 106, No. 36, 2002*

Pettersson et al.

If we use $d = 2\pi w_0^2/\lambda$, namely the Rayleigh length appropriate for the beam profile in air, we obtain:

$$\tan(\alpha) = \frac{2\pi w_0}{\lambda}\left(\frac{\delta n}{n^2}\right)Z \qquad (11)$$

For $w_0 = 15$ μm and $\lambda = 0.4$ μm, a divergence angle of 12 mrad can be expected. This is comparable to the divergence of the beam due to the lens (fl = 15 cm, beam diameter of 0.4 cm). The effect can be significantly larger if the beam has undergone self-focusing, where now d in eq 10 can become significantly larger than its confocal value.

The effects of the third-order susceptibility of the un-ionized liquid and the three-photon induced plasma can be combined to obtain the governing intensity dependence of photorefraction:

$$n = n_0 + n_2I + \delta n_e(I) = n_0 + n_2I - n_eI^3 \qquad (12)$$

in which n_e is chosen positive to clearly highlight the counter effects of bound and free electrons. The equation clearly contains the necessary physics to explain the observed intensity dependence of the transmission data. At low intensity, the third-order susceptibility of the bound electrons induces self-focusing. As ionization sets in, the free electrons start to contribute to the index. At $n_2 = n_eI^2$, the self-focusing is completely compensated by defocusing. A further increase in electron density would lead to divergence of the transmitted beam. However, this is a self-limiting process. As the beam expands, its intensity drops, and therefore the density of photogenerated electrons drops even faster. As such, the process will be bounded by the linear transmission curve, as observed in Figure 5. The repetition of the entire process at higher intensity we attribute to the multi-mode nature of the pump beam. The first sharp focusing—defocusing process is attributed to the central Gaussian mode, and the secondary peak to the surrounding higher order modes. Indeed, both laser mode structure and nonlinearities of the medium are possible to obtain quantitatively through transmission measurements using thin samples in the so-called z-scan technique.[60]

The exact analysis of the propagation of the multi-mode laser beam subject to attenuation and the nonlinearities in eq 12, is beyond the scope of the present work. However, a qualitative analysis is useful to establish consistency of the proposed model, and as an independent estimate of the photogenerated electron density. The self-focusing length due to $\chi^{(3)}$ can be approximated as $z_f = w_0(n_0/n_2I)^{1/2}$. Assuming that this shifts the vertex of the cone for the transmitted beam, the transmitted intensity I_{out} may be related to the weak field limit I_{in} through:

$$I_{out} = I_{in}\frac{h^2}{(h - z_f)^2} = I_{in}\frac{h^2}{[h - w_0(n_0/n_2I)^{1/2}]^2} \qquad (13)$$

in which h is the distance between the weak field focus and the limiting aperture plane of the detector. The observed initial self-focusing can be fit with this expression using $n_2 = 1.5 \times 10^{-18}$ cm^2 W^{-1} (1.5×10^{-11} esu) as shown in Figure 5. The associated value of z_f is 2 cm, consistent with visual inspections. The turnover in the transmission can be expected from the condition $n_2I = n_eI^3$ in eq 12, where now the intensity in the self-focused volume is needed. Using the diffraction limit for the focal waist, $N_e = 10^{18}$ cm^{-3} can be retrieved for the turnover region. Note, under these conditions the divergence angle due to the negative dispersion in the plasma is obtained by setting $d = z_f$ in eq 10, and by replacing w_0 by $w_0/\sqrt{3}$, namely by considering the

beam waist over which I^3 drops to half its value. The divergence angle now increases to $\sim$100 mrad, namely an order of magnitude larger than its value in the absence of self-focusing. This nicely rationalizes the observed intensity profile of the transmission in Figure 5.

D. The Absence of Gain. A major motivation of the present work was the investigation of strong-field pumping as a means of obtaining gain on the excitonic transitions. We have searched for evidence of gain in the form of spectral narrowing of the on-axis fluorescence, and have failed to do so in both solid and liquid samples, at all pump intensities. The reasons for this failure are not clear in view of the system parameters, which deserve scrutiny.

The stimulated emission cross-section for the excitonic transition is given as

$$\sigma = \frac{n\lambda^4}{8\pi c\tau\Delta\lambda} \qquad (14)$$

We consider only the B-state component of the Xe$_2$* which has a large enough cross-section to be a proper laser candidate.[36] Inserting the values $\lambda = 172$ nm, $\tau = 1.3$ ns,[23] and $\Delta\lambda = 7$ nm yields $\sigma = 2.6 \times 10^{-16}$ cm^2. To observe a 10% reduction in the line width in a single-pass, the product of the exciton number density and the gain length must be $Nl \sim 2 \times 10^{16}$ cm^{-2} (e.g. and 2×10^{17} cm^{-3} over a length of 1 mm). Although the physical length of our sample is 1 cm in the solid and 2 cm in the liquid, the effective path lengths over which the peak densities of excited states can be generated depends strongly on the nonlinearities that define the profile of the pump. In the absence of self-refraction, based on the MPI cross-sections, we estimated an electron–hole pair density–length product of $N_el = 1.4 \times 10^{16}$cm^{-2} in the liquid phase ($N_e = 10^{17}$ cm^{-3}, $\Delta x_{1/2} = 0.14$ cm), and 4.5×10^{16} cm^{-2} in the solid state ($N_e = 10^{19}$ cm^{-3}, $\Delta x_{1/2} = 45$ μm). These may be regarded as lower limits, since self-focusing increases both the density and gain length. From the self-refraction analysis we estimated a density–length product of $N_el = 10^{17} - 10^{18}$ cm^{-2}. In the absence of loss mechanisms, the electron–hole pairs must recombine to populate all self-trapped states. If we assume a statistical ratio of 1:3 between the A and B states, and take into account that in the solid (but not in the liquid) there are two sites, then only $\sim$35% of the initial pairs are useful for gain. This leaves us nearly an order of magnitude above the required number densities to observe spectral narrowing. Other loss channels, which have been carefully considered before, are exciton–exciton annihilation and reabsorption.[36] The former will greatly depend on the mobility of excitons, which in the solid state is controlled by the crystallinity of the sample. A measure of this is provided by the relative contributions of emission from free and self-trapped excitons.[25] Zimmerer et al. were able to grow crystals where the integrated intensity of the free and trapped exciton bands are similar. In our solid samples, the intensity of the free exciton band was always a small fraction of the trapped exciton, indicating fast trapping, and therefore reduced mobility and loss. These considerations are unimportant for the liquid case, where the trapping rates must be greater than 10^{12} s^{-1}. Although, in the liquid diffusion controlled encounters of the trapped excitons can lead to annihilation, given the radiative lifetime of the excimer of 10^{-9} s, this loss channel can only become significant at excitonic densities above 10^{19} cm^{-3}. Of the intrinsic loss mechanisms, we are left with reabsorption, which has been invoked as the main reason for the failure to observe net gain in electron-beam-pumped solids.[36] Note, the present analysis is based on pump intensities where the turnover

Strong-Field Excitation of Liquid and Solid Xe

J. Phys. Chem. A, Vol. 106, No. 36, 2002 **8315**

in the power dependence of fluorescence is observed. Pumping above this limit would seem ineffective in increasing the density−length product. A quantitative understanding of this saturation behavior would be valuable in optimizing pumping geometries. The present arrangement does not produce a measurable spectral narrowing, and therefore of gain.

V. Conclusions

The intense fields generated with focused femtosecond pulses provide an efficient method for nonresonant access to excitonic states in condensed Xe. The excitation mechanism, using 60 fs pulses, changes from multiphoton to field-induced tunneling between 400 and 800 nm, respectively. In essence, field-induced tunneling threshold occurs at intensities below the required six-photon excitation in the case of pumping at 800 nm. At both wavelengths, the formation of excitons can be attributed to strong-field-induced ionization, and subsequent electron−hole recombination. Despite pumping at intensities above the saturation of the power law behavior for ionization, dielectric breakdown cannot be induced. This self-limiting behavior is understood through explicit simulations of the field-coupled electron kinetics. By numerically solving the Fokker−Planck equations governing the evolution of the electron energy distribution during the laser pulse, it is discovered that the distribution localizes at the Ramsauer-Townsend minimum, near 0.7 eV. This prevents the generation of secondaries through impact ionization and precludes the possibility of an electron avalanche, which describes breakdown in liquid helium. The combination of attenuation of the pump beam in the stagnant plasma, and its divergence due to the negative dispersion of the plasma, explain the self-limiting behavior of the ionization. This phenomenon in itself is quite interesting as an optical limiter for high intensities, distinct from the more common mechanism of reverse saturable absorbers.[61] Prior to saturation of the process, self-focusing of the 400 nm pump beam is observed, and understood in terms of the third-order nonlinear susceptibility of the bulk. It is estimated, based on known multiphoton ionization cross-sections and based on the plasma-induced defocusing, that ionization densities as high as 10^{19} cm^{-3} are reached. Even after taking intrinsic loss mechanisms into account, and particularly in the self-focused stage of pumping, the density−length product of excitons formed through electron−hole recombination is sufficient to attain gain over the excitonic VUV transition. Nevertheless, the spectral profile of the transition does not show any evidence of gain. This could indicate that reabsorption by the excitons has a larger cross-section than that of stimulated emission, which at 10^{-16} cm^2 is quite high. Otherwise, we must conclude that not all system parameters are well understood in this strongly nonlinear system. A quantitative analysis of the nonlinear propagation of radiation under strong pumping conditions in this system would be quite valuable.

References and Notes

(1) Perry, M. D.; Mourou, G. *Science* **1994**, *264*, 917.

(2) Corkum, P. B.; Ivanov, M. Y.; Wright, J. S. *Annu. Rev. Phys. Chem.* **1997**, *48*, 387.

(3) Keldysh, L. V. *Sov. Phys.-JETP* **1965**, *20*, 137.

(4) Augst, S.; Meyerhofer, D. D.; Strickland, D.; Chin, S. L. *J. Opt. Soc. Am.* **1991**, *B8*, 858.

(5) Chang, Z. H.; Rundquist, A.; Wang, H. W.; Murnane, M. M.; Kapteyn, H. C. *Phys. Rev. Lett.* **1999**, *82*, 2006.

(6) Christov, I. P.; Murnane, M. M.; Kapteyn, H. C. *Phys. Rev. Lett.* **1997**, *78*, 1251.

(7) *Molecules in Laser Fields;* Bandrauk, A. D., Ed.; M. Dekker: New York, 1994.

(8) Ledingham, K. W. D.; Singhal, R. P. *Int. J. Mass Spectrom. Ion Process.* **1997**, *163*, 149.

(9) Levis, R. J.; Menkir, G. M.; Rabitz, H. *Science* **2001**, *292*, 709.

(10) Karczmarek, J.; Wright, J.; Corkum, P.; Ivanov, M. *Phys. Rev. Lett.* **1999**, *82*, 3420.

(11) Snyder, E. M.; Buzza, S. A.; Castleman, A. W., Jr. *Phys. Rev. Lett.* **1996**, *77*, 3347.

(12) Purnell, J.; Snyder, E. M.; Wei, S.; Castleman, A. W., Jr. *Chem. Phys. Lett.* **1994**, *229*, 333.

(13) Ditmire, T.; Zweiback, J.; Yanovsky, V. P.; Cowan, T. E.; Hays, G.; Wharton, K. B. *Nature* **1999**, *398*, 489.

(14) Shen, Y. R. *The Principles of Nonlinear Optics*; Wiley-Interscience: New York, 1984.

(15) *The Supercontinuum Laser Source*; Alfano, R. R., Ed.; Springer-Verlag: New York, 1989.

(16) Stuart, B. C.; Feit, M. D.; Herman, S.; Rubenchik, A. M.; Shore, B. W.; Perry, M. D. *Phys. Rev. B* **1996**, *53*, 1749.

(17) Benderskii, A. V.; Zadoyan, R.; Schwentner, N.; Apkarian, V. A. *J. Chem. Phys.* **1999**, *110*, 1542.

(18) Sliwinski, G.; Sawczak, M.; Schwentner, N. *J. Low Temp. Phys.* **2001**, *122*, 485.

(19) Apkarian, V. A.; Schwentner, N. *Chem. Rev.* **1999**, *99*, 1481.

(20) Fugol, I. Ya. *Adv. Phys.* **1978**, *27*, 1.

(21) Fugol, I. Ya. *Adv. Phys.* **1988**, *37*, 1.

(22) Schwentner, N.; Koch, E. E.; Jortner, J. *Electronic Excitations in Condensed Rare Gases*; Springer-Verlag: Berlin, 1985.

(23) Zimmerer, G. In *Excited-state Spectroscopy in Solids;* Grassano, U. M., Terzi, N., Eds.; North-Holland: Amsterdam, 1987.

(24) Song, K. S.; Williams, R. T. *Self-Trapped Excitons*, 2nd ed.; Springer Series in Solid-State Sciences; Springer-Verlag: Berlin, 1996; Vol. 105.

(25) Varding, D.; Becker, J.; Frankenstein, L.; Peters, B.; Runne, M.; Schröder, A.; Zimmerer, G. *Low Temp. Phys.* **1993**, *19*, 427.

(26) Varding, D.; Reimand, I.; Zimmerer, G. *Phys. Rev. Status Solidi B* **1994**, *185*, 301.

(27) Steeg, B.; Gminder, E.; Kirm, M.; Kisand, V.; Vielhauer, S.; Zimmerer G. *J. Electron Spectrosc. Relat. Phenom.* **1999**, *101−103*, 879.

(28) Reimand, I.; Gminder, E.; Kirm, M.; Kisand, V.; Steeg, B.; Varding, D.; Zimmerer, G. *Phys. Status Solidi B* **1999**, *214*, 81.

(29) Peterson, E. S.; Schwartz, B. J.; Harris, C. B. *J. Chem. Phys.* **1993**, *99*, 1693.

(30) Jortner, J.; Meyer, L.; Rice, S. A.; Wilson, E. G. *J. Chem. Phys.* **1965**, *42*, 4250.

(31) Basov, N. G.; Danilychev, V. A.; Popov, Yu. M.; Khodkevich, D. D. *JETP Lett.* **1970**, *12*, 329.

(32) Rhodes, C. K. *Excimer Lasers*; Topics in Applied Physics; Springer-Verlag: Berlin, 1979; Vol. 30.

(33) Koehler, H. A.; Ferderber, L. J.; Redhead, D. L.; Ebert, P. J. *Appl. Phys. Lett.* **1972**, *21*, 198.

(34) Turner, C. E., Jr. *Appl. Phys. Lett.* **1977**, *31*, 659.

(35) Loree, T. R.; Showalter, R. R.; Johnson, T. M.; Birmingham, B. S.; Hughes, W. M. *Opt. Lett.* **1989**, *14*, 1051.

(36) Nahme, H.; Schwentner, N. *Appl. Phys.* **1990**, *B51*, 177.

(37) Shahidi, M.; Jara, H.; Pummer, H.; Egger, H.; Rhodes, C. K. *Opt. Lett.* **1985**, *10*, 448.

(38) Schwentner, N.; Apkarian, V. A. *Chem. Phys. Lett.* **1989**, *154*, 413.

(39) Frankowski, M.; Sliwinski, G.; Schwentner, N. *J. Low Temp. Phys.* **2001**, *122*, 443.

(40) Freeman, D. E.; Yoshino, K.; Tanaka, Y. *J. Chem. Phys.* **1974**, *61*, 4880.

(41) Lipson, R. H.; LaRocque, P. E.; Stoicheff, B. P. *J. Chem. Phys.* **1985**, *82*, 4470.

(42) Hahn, U.; Schwentner, N.; Zimmerer, G. *Opt. Commun.* **1977**, *21*, 237.

(43) Fugol, I. Ya.; Ogurtsov, A. N.; Grigorashchenko, O. N.; Savchenko, E. V. *Sov. J. Low Temp. Phys.* **1992**, *18* (1), 27.

(44) Kink, R.; Lohmus, A.; Selg, M. *Phys. Status Solidi B* **1981**, *107*, 479.

(45) Kink, M.; Kink, R.; Kisand, V.; Maksimov, J.; Selg, M. *Nucl. Instrum. Methods Phys. Res. B* **1997**, *122*, 668.

(46) DeWitt, M. J.; Lewis, R. J. *J. Chem. Phys.* **1998**, *108*, 7739.

(47) Gibson, G.; Luk, T. S.; Rhodes, C. K. *Phys. Rev. A* **1990**, *41*, 5049.

(48) Zel'dovich, Ya. B.; Raiser, Yu. P. *Sov. Phys. JETP* **1965**, *20*, 772.

(49) Uiterwaal, C. J. G. J.; Xenakis, D.; Charalambidis, D.; Maragakis, P.; Schröder, H.; Lambropoulos, P. *Phys. Rev. A* **1998**, *57*, 392.

(50) Perry, M. D.; Landen, O. L.; Szöke, A.; Campbell, E. M. *Phys. Rev. A* **1988**, *37*, 747.

(51) Van Hove, L. *Phys. Rev.* **1954**, *95*, 249.

(52) Cohen, M. H.; Lekner, J. *Phys. Rev.* **1967**, *158*, 35.

(53) Lekner, J. *Phys. Rev.* **1967**, *158*, 130.

(54) Gushchin, E. M.; Kruglov, A. A.; Obodovskii, I. M. *Sov. Phys. JETP* **1982**, *55* (4)*,* 650.

(55) Jones, H. M.; Kunhardt, E. E. *Phys. Rev. B* **1993**, *48*, 9382.

(56) Wetzel, R. C.; Baiocchi, F. A.; Hayes, T. R.; Freund, R. S. *Phys. Rev. A* **1987**, *35*, 559.

(57) Frost, L. S.; Phelps, A. V. *Phys. Rev.* **1964**, *136*, A1538.

(58) Akhmanov, S. A.; Khokhlov, R. V.; Sukhorukov, A. P. In *Laser Handook*; Arechhi, F. T., Schulz-Dubois, E. O., Eds.; North-Holland: Amsterdam, 1972; Vol. 2, pp 1151−1228.

(59) Shelton, D. P. *Phys. Rev. A* **1990**, *42*, 2578.

(60) Sheik-Bahae, M.; Said, A. A.; Wei, T. H.; Hagan, D. J.; Stryland, E. W. *IEEE J. Quantum Electron.* **1990**, *26*, 760; Said, A. A.; Sheik-Bahae, M.; Hagan, D. J.; Wei, T. H.; Wong, J.; Young, J.; Stryland, E. W. *J. Opt. Soc. Am. B* **1992***, 9*, 405.

(61) Miles, P. A. *Appl. Opt*. **1994**, *33*, 6965.